Topologically protected Dirac cones in compressed bulk black phosphorus

Ruixiang Fei, Vy Tran, and Li Yang
Department of Physics, Washington University in St. Louis, St. Louis, Missouri 63130, USA
(Received 21 January 2015; revised manuscript received 11 May 2015; published 27 May 2015)

Using the $k \cdot p$ theory and first-principles simulations, we predict that applying a moderate uniaxial or hydrostatic pressure (>0.6 GPa) on bulk or multilayer black phosphorus (BP) can diminish its bandgap and produce one-dimensional and even two-dimensional (2D) Dirac cones. Similar to topological insulators, these 2D Dirac cones result from two competing mechanisms: the unique linear band dispersion tends to open a gap via a "pseudo-spin-orbit" coupling, while the band symmetries preserve the material's gapless spectrum. In particular, these Dirac cones in BP are bulk states that do not require time-reversal symmetry, thus they can keep the high carrier mobility even in the presence of surface or magnetic perturbations. Finally, our predictions can be detected by the material's unusual Landau levels.

DOI: 10.1103/PhysRevB.91.195319 PACS number(s): 73.22.−f, 71.15.−m

I. INTRODUCTION

To date, Dirac materials, such as graphene [1,2], topological insulators (TIs) [3–5] or spin Hall insulators (SHIs) [6,7], topological crystalline insulators (TCIs) [8,9], and Weyl semimetals (WSs) [10,11], have drawn tremendous research interest. Graphene hosts two-dimensional (2D) Dirac fermions [12,13]; TIs are materials with a bulk energy gap but possess gapless two-dimensional (2D) Dirac surface states protected by time-reversal symmetry [14,15]; TCIs exhibit metallic surface states protected by the mirror symmetry [9]; WSs, which are protected by crystal symmetries, exhibit energy overlaps that occur at isolated points in momentum space where the linear bands cross at the Fermi level [10]. The impact and implications of these materials are difficult to overstate. The discovery of the anomalous Hall effect [16,17], the fractional Hall effect [18], chiral anomaly [19,20], and Majorana fermions [21,22], to name a few, have inspired enormous efforts in the search for new Dirac materials.

Recently a new type of 2D semiconductor, few-layer black phosphorus (BP) (phosphorene), has been fabricated [23–25]. It exhibits promising carrier mobilities and unique anisotropic transport, optical, and thermal properties [23–30]. In particular, few-layer BP possess a unique band structure, whose dispersion is nearly linear along the armchair direction but parabolic along other directions [31,32]. An obvious idea follows from this unique structure: if one can significantly reduce the bandgap or even achieve the band inversion, novel features may result, e.g., the formation of Dirac cones. However, the bandgap of monolayer and few-layer BP is significant (up to 2.2 eV) [26,29,33], making it impractical to close. Alternatively, bulk black or thick multilayer phosphorus has a much smaller bandgap, only around 300 meV [26,34], which is more tractable.

In this work, we show that the $k \cdot p$ Hamiltonian of bulk BP can be written as the free-electron one with off-diagonal terms which take on the same form as the Rashba and Dressehaus spin-orbit coupling (SOC). Thus we deem this off-diagonal interaction "pseudo-spin-orbit" coupling (PSOC). If the band inversion is realized, PSOC tends to open a gap. However, similar to TIs, the band symmetry requires a gapless spectrum. The competition between PSOC and band symmetry causes the Fermi surface to undergo a topological transition from a sphere to a ring of 2D Dirac cones. Using first-principles simulations, we show that pressure can be an efficient tool to realize these 2D and even 1D Dirac cones. We further find that the intensity of PSOC is more than an order of magnitude larger than typical SOC, making it promising to realize extremely enhanced SOC effects in light-element materials. On the other hand, unlike TIs, because our predicted Dirac cones do not require the time-reversal symmetry, they are robust in the presence of magnetic fields. Thus this unique electronic structure can be verified by the unusual energy scaling law exhibited by Landau levels.

The remainder of this paper is organized as follows: in Sec. II we introduce the atomic structures of our calculated BP; in Sec. III the effective Hamiltonian and $k \cdot p$ model are presented and the pseudo-spin-orbit coupling is discussed; in Sec. IV we discuss the band inversion and the formation of Dirac cones in BP; in Sec. V the first-principles simulations show that applying moderate pressure can realize the band inversion and Dirac cones; in Sec. VI the corresponding Landau levels are presented for compressed BP; in Sec. VII we summarize our studies and present conclusions.

II. ATOMIC STRUCTURES

The atomic structure of bulk BP is plotted in Figs. 1(a) and 1(b). Here we use a simple orthorhombic conventional unit cell, which is twice the size of the primitive cell. The corresponding first Brillouin zone (BZ) is shown in Fig. 1(c). The double-cell procedure simply folds the first BZ and this is convenient for the following presentation. The bulk BP atomic structures are fully relaxed according to density functional theory (DFT) with the Perdew, Burke, and Ernzerhof (PBE) functional associated with van der Waals corrections [35,36]. Because DFT underestimates bandgaps, we use a hybrid functional theory (HFT), HSE06 [37,38], to calculate band structures, which is in good agreement with the GW calculations and experiments of bulk BP [26,34].

III. THE EFFECTIVE HAMILTONIAN MODEL AND PSEUDO-SPIN-ORBIT COUPLING

We begin with the widely used $k \cdot p$ model to capture the BP's electronic structure. The C_{2h} point group invariance

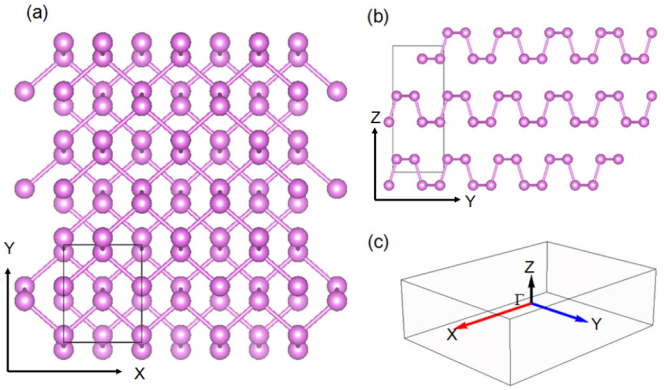

FIG. 1. (Color online) (a) Top view of the atomic structure of bulk BP. The unit cell and lattice vectors are marked. The zigzag and armchair directions are illustrated as well. (b) Side view of BP. (c) The first BZ.

allows us to describe BP using a two-band model [39,40]. The low-energy effective Hamiltonian is

$$H = \begin{pmatrix} E_c + \alpha k_x^2 + \beta k_y^2 + \gamma k_z^2 & v_f k_y \\ v_f k_y & E_v - \lambda k_x^2 - \mu k_y^2 - \nu k_z^2, \end{pmatrix}, \quad (1)$$

where k_x, k_y, and k_z are components of the crystal momentum along the x, y, and z directions, respectively. The conduction and valance band energies, $E_c = 0.15$ eV and $E_v = -0.15$ eV, are set to fit the bulk bandgap (300 meV). $\alpha = 0.036$ eV nm^2, $\beta = 0.253$ eV nm^2, $\gamma = 0.131$ eV nm^2, $\lambda = 0.054$ eV nm^2, $\mu = 0.313$ eV nm^2, and $\nu = 0.063$ eV nm^2 are fitted parameters that describe the band edge curvature, and $v_f = 3.5 \times 10^5$ m/s is the Fermi velocity of the nearly linear band along the armchair (y) direction. By fitting these parameters, as shown in Figs. 2(a) and 2(b), the $k \cdot p$ result nearly perfectly matches that of the first-principles HSE06 calculations.

The special characteristics of Eq. (1) are the off-diagonal terms, which produce the linear dispersion along the armchair (y) direction, as shown in Fig. 2(a). In fact, this off-diagonal interaction can be split into two terms,

$$\begin{aligned} H_{\text{off}} &= H_{DSOC} + H_{RSOC} \\ &= 1/2\, v_f(k_x\sigma_y + k_y\sigma_x) - 1/2\, v_f(k_x\sigma_y - k_y\sigma_x), \end{aligned} \quad (2)$$

where σ_x and σ_y are Pauli matrices. Interestingly, these two terms (H_{DSOC} and H_{RSOC}) have the forms of the Dressehaus and Rashba SOCs [41], respectively. Realistically, Dressehaus and Rashba SOCs cannot exist in intrinsic bulk BP because of the inversion symmetry. Hence we call these interactions PSOC. Impressively, the PSOC strength parameter v_f of BP is one to two orders of magnitude larger than that of typical SOC [42]. It is thus attractive to mimic superstrong SOC effects in light-element materials with this PSOC. This is similar to the work about the strain-induced pseudomagnetic field in graphene [43]. Furthermore, considering the dramatic effect of SOC in TIs, it is natural to expect that diminishing or inverting the bandgap in bulk BP with PSOC will produce novel electronic characteristics. More insightful studies on PSOC will be important for further studies of BP and many other 2D materials.

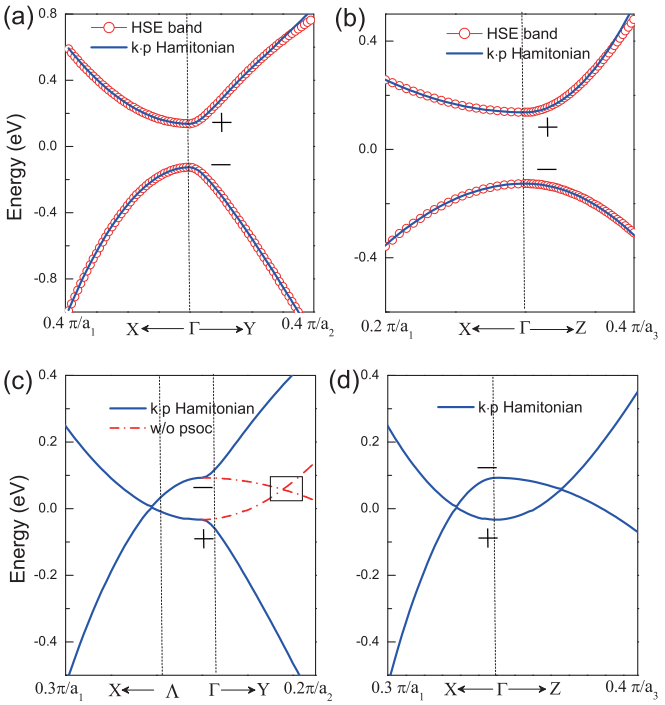

FIG. 2. (Color online) (a) and (b) are the band structures of intrinsic BP. The red dots are from the HSE06 simulation and the blue line is from $k \cdot p$ calculations. (c) and (d) are the band structures calculated from the $k \cdot p$ calculations under the band-inversion condition. The dashed lines in (c) are the $k \cdot p$ result without including the PSOC interaction [the off-diagonal term in Eq. (1)]. The parities ($+/-$) are marked as well.

IV. BAND INVERSION AND THE FORMATION OF DIRAC CONES

It is easy to mimic the band inversion in the $k \cdot p$ model: one simply assigns the valence band edge energy E_v a higher value than the conduction band edge energy E_c in Eq. (1). Surprisingly, instead of producing simple band overlaps, we observe an unusual topological transition at the Fermi surface. In Figs. 2(c) and 2(d), the band crossing at the Γ-Y axis is opened by the PSOC, while the band crossing is preserved at the K point along the Γ-X direction. As a result, 2D graphene-like Dirac cones are formed and the schematic 3D plots are presented in Figs. 3(a)–3(c) for three specific cutting planes, X-Y, Y-Z, and X-Z, respectively. The linear band dispersions and Dirac cones are observed in both X-Y and Y-Z planes and a ring-like band crossing occurs in the X-Z plane. Actually, any point on the ring of Fig. 3(c) corresponds to a Dirac cone in other 2D planes. In Fig. 3(d), we show that this ring-like band crossing continuously evolves to a pair of Dirac cones by varying the tilting angles from the X-Z plane to the Y-Z plane. In other words, the set of tilting angles that do not exhibit these Dirac cones is of measure zero.

The mechanisms responsible for forming the ring of Dirac cones are similar to those in TIs, but there are crucial differences. First, similar to the band inversion and gap opening

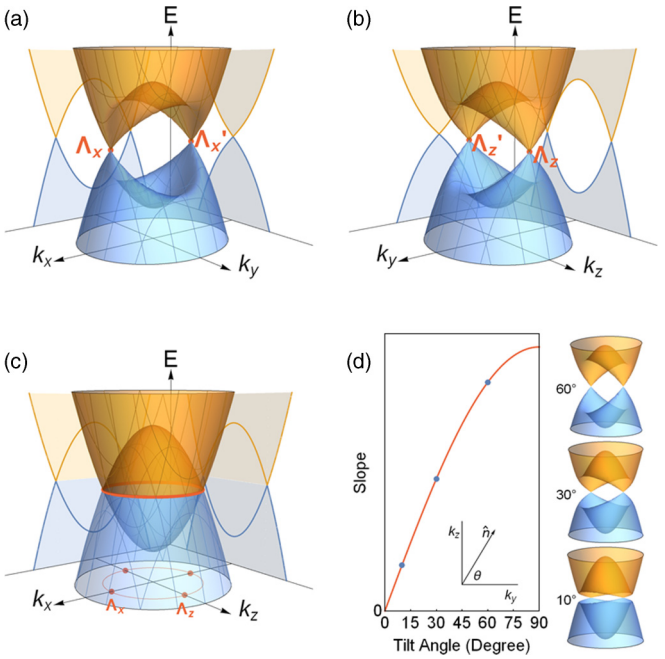

FIG. 3. (Color online) The 3D band structures of BP of the X-Y plane (a), the Y-Z plane (b), and the X-Z plane (c). The band overlap in (c) forms a ring structure. (d) The schematic evolution of the band structure and band slope from the X-Z plane to the X-Y plane via changing of the tilted angle.

that occurs in TIs due to SOC, the gap opening in Fig. 2(c) is from the PSOC. For comparison, the dashed lines in Fig. 2(c) exclude PSOC and thus the bands trivially cross each other as marked by the square. Second, the gap of BP is not completely opened: the valence and conduction bands still touch at the K point [Fig. 2(c)] or by the ring [Fig. 3(c)]. This gapless feature is guaranteed by a symmetry constraint based on two facts: the bottom conduction band is formed by what was originally the top valence band prior to the band inversion and the parity symmetries of the top of the valence band and the bottom of the conduction band are inverse to each other, as shown in Fig 2. Therefore, contact between the conduction and valence bands is required to provide a continuous symmetry evolution. This mechanism is similar to the one responsible for forming gapless surface states in TIs [44]. However, there are no surface states in our calculated bulk BP, thus it is the bulk valence and conduction bands that must touch, resulting a Dirac semimetal instead of insulators.

Further symmetry analysis shows that compressed BP can be a promising, strong TI if the inversion symmetry is broken. In our centrosymmetry structure, there are eight distinct time-reversal invariant momenta (TRIM), which can be expressed in terms of primitive reciprocal lattice vectors as $K_{i=n_1n_2n_3} = (n_1b_1 + n_2b_2 + n_3b_3)/2$, with $n_j = 0,1$. Following the definition of Ref. [5], because the band inversion is induced by PSOC only at the Γ point, not at the other TRIM, we find that four Z_2 indices of compressed BP are 1; (100), which is the sign for potentially strong TIs. This is evidenced by a recent work [45], in which breaking the inversion symmetry in few-layer BP produces surface topological states.

Following the above analysis of the $k \cdot p$ model, 3D Weyl points can exist if the x direction also exhibits an off-diagonal linear term. We found that the lack of linear band dispersion along the Γ-X direction is caused by the mirror symmetry across the Y-Z plane in BP's crystal structure. One may search for WSs by looking for structures without that mirror symmetry. Then the band inversion may give hope for 3D Weyl points.

V. FIRST-PRINCIPLES CALCULATIONS

Beyond the $k \cdot p$ model, an obvious question is how one can practically achieve band inversion in BP. Towards this end, we turn to the first-principles simulations for quantitative answers. Our HSE06 calculations show that applying an external pressure along the y (armchair) or x (zigzag) direction produces promising effects (see the Supplemental Material [46]). Note that BP is much softer along the y (armchair) direction because of its anisotropic atomic structure [47]. We also find that the armchair pressure is more efficient to tune the bandgap. Combining these two factors, we focus on the armchair uniaxial pressure. However, for experiments, a similar effect will be observed for hydrodynamic pressure because of the much softer modulus along the armchair direction.

First, an applied critical armchair pressure (0.6 GPa) diminishes the bandgap and produces a 1D Dirac cone along the Γ-X direction. This pressure is well within the capability of current experiments [48,49]. Under this pressure, BP simultaneously contains both classical mass carriers and

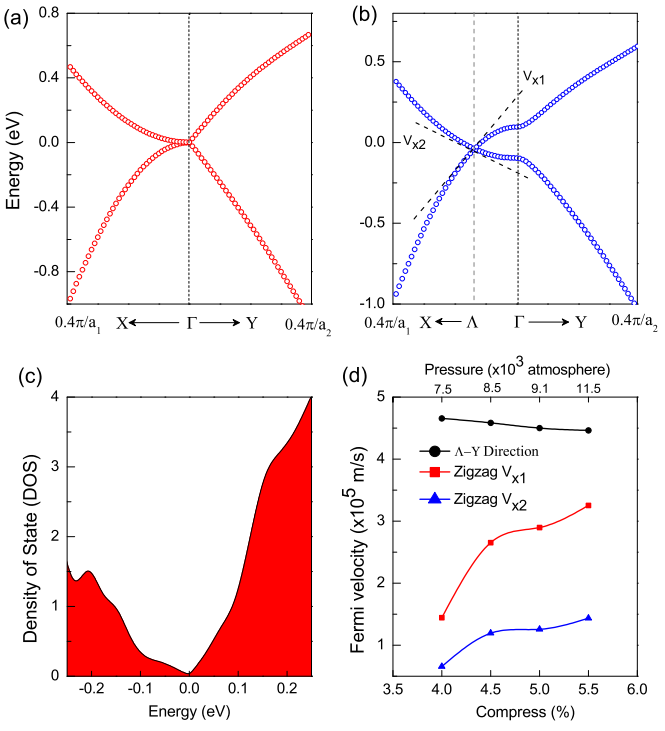

FIG. 4. (Color online) (a) The HSE06-calculated band structure of BP under the critical armchair pressure (0.6 GPa). (b) The HSE06-calculated band structure of BP under 0.9 GPa armchair pressure. The black dashed line represents the Fermi velocity. (c) The density of state (DOS) of BP under 0.9 GPa armchair pressure. (d) The anisotropic fermi velocity of electrons and holes of 2D Dirac cones varied with the armchair pressure; the zigzag direction Fermi velocities V_{x1}, V_{x2} are shown in (b).

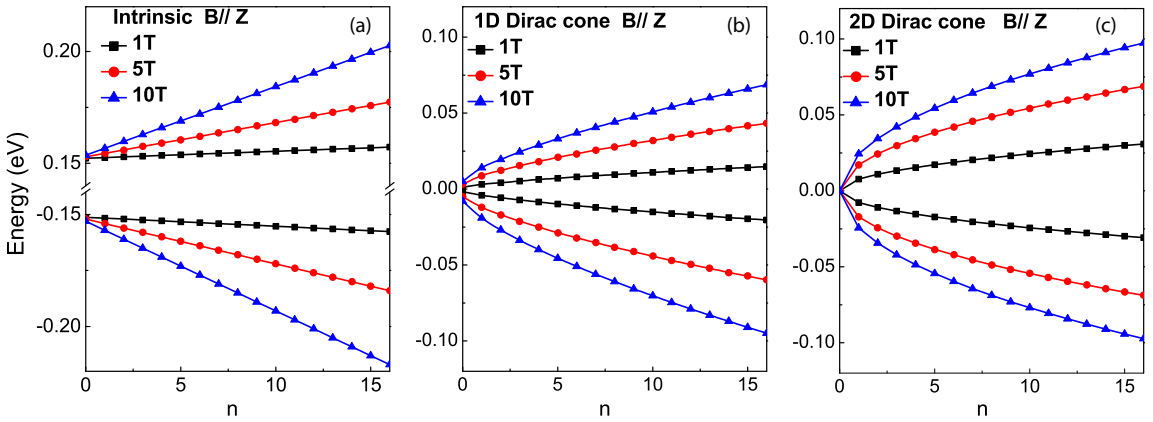

FIG. 5. (Color online) (a) The energy spectrum of Landau levels (index n) of intrinsic BP with magnetic field; (b) that under the critical pressure (0.6 GPa), in which the 1D Dirac cone is formed; (c) that under a pressure of 0.9 GPa, in which 2D Dirac cones are formed.

Dirac fermions, making it interesting for observation of many unusual phenomena, such as unconventional Landau levels and unique plasmon behaviors. Moreover, as discussed in supplementary information, the effective mass is significantly reduced by forming Dirac cones, giving hope to higher carrier mobility and device applications.

Second, larger pressures can create a band inversion. Similar to the $k \cdot p$ theory predictions, a pressure of 0.9 GPa yields a band crossing at the Γ point and 2D Dirac cones are formed, as shown in Fig. 4(b). The corresponding density of states (DOS) is shown in Fig. 4(c). We can clearly see a linear DOS in the low-energy regime, which is similar to graphene and can be identified by a constant optical absorbance [50]. Obviously, the Fermi velocities of compressed BP must be anisotropic as well and can be efficiently tuned by varying the applied pressure, as concluded in Fig. 4(d). Finally, the atomic structure's high symmetry and these Dirac cones are robust under random distortions (Supplemental Information).

VI. LANDAU LEVELS IN COMPRESSED BP

Because Dirac cone states in BP are robust even in the face of broken time-reversal symmetry, we propose that the evolution of the electronic structure from conventional semiconductors to one possessing 1D Dirac cones and 2D Dirac cones can be observed by measuring the energy spectrum of Landau levels. For example, considering the X-Y plane, before reaching the critical point for closing the bandgap, the energy spectrum of the Landau levels is that of a typical semiconductor, i.e., it is linear with the level index, as shown in Fig. 5(a):

$$\begin{aligned} E &= E_c + (n + 1/2)\hbar\omega_c, \\ E &= E_v - (n + 1/2)\hbar\omega_v, \end{aligned} \tag{3}$$

where ω_c and ω_v are the cyclotron frequencies of electrons and holes, respectively. Importantly, there is no zero-energy solution for this case.

At the critical pressure (0.6 GPa), because of the perfectly 1D linear band dispersion along the Γ-Y direction [Fig. 4(a)], the effective Hamiltonian with the magnetic field introduced by the Landau gauge $\overrightarrow{A} = (-By,0,0)$ is

$$\begin{aligned} \frac{1}{2m_c}(\hbar k_x - eBy)^2\phi_A - i\hbar v_f \frac{d}{dy}\phi_B &= E\phi_A, \\ -\frac{1}{2m_v}(\hbar k_x - eBy)^2\phi_B - i\hbar v_f \frac{d}{dy}\phi_A &= E\phi_B, \end{aligned} \tag{4}$$

where $v_f = 3.5 \times 10^5$ m/s is the Fermi velocity obtained from HSE06 simulations. The corresponding energy spectrum of Landau levels in a magnetic field is presented in Fig. 5(b), which deviates from the linear relation of Fig. 5(a). Finally, for higher pressures that form 2D Dirac cones, the Landau levels follow the well-known square-root dependence [2,12], $E_n \propto \sqrt{n}$, and exhibit a unique zero-energy solution, as shown in Fig. 5(c).

VII. SUMMARY

In conclusion, we predict that applying a moderate pressure (>0.6 GPa) on bulk BP can dramatically reshape its band structure. Namely, its bandgap will close and band inversion will induce a topological semimetal via the so-called PSOC interaction. The formed 1D or 2D Dirac cones exhibit tunable anisotropic Fermi velocities and compressed BP thus may uniquely integrate both massless Dirac Fermions and massive classical carriers. Our proposed PSOC can realize superenhanced SOC effects in many structures without heavy elements. Furthermore, these bulk Dirac-cone states are robust even under broken time-reversal symmetry and they can be identified by our calculated unusual Landau levels.

Note added. During the reviewing process, our predicted Dirac cones in compressed BP were observed in a recent experiment [51].

ACKNOWLEDGMENTS

We acknowledge fruitful discussions with Li Chen, Shiyuan Gao, Zohar Nussinov, and Ryan Soklaski. This work is supported by the National Science Foundation Grant No. DMR-1207141. The computational resources were provided by the Lonestar and Stampede of Teragrid at the Texas Advanced Computing Center (TACC) and the Edison cluster of the National Energy Research Scientific Computing Center (NERSC). The first-principles calculation was performed with the Vienna *ab initio* simulation package (VASP) [52].

[1] K. S. Novoselov, A. K. Geim, S. V. Morozov, D. Jiang, M. I. Katsnelson, I. V. Grigorieva, S. V. Dubonos, and A. A. Firsov, Nature (London) **438**, 197 (2005).

[2] Y. Zhang, Y.-W. Tan, H. L. Stormer, and P. Kim, Nature (London) **438**, 201 (2005).

[3] Y. L. Chen, J. G. Analytis, J.-H. Chu, Z. K. Liu, S.-K. Mo, X. L. Qi, H. J. Zhang, D. H. Lu, X. Dai, Z. Fang, S. C. Zhang, I. R. Fisher, Z. Hussain, and Z.-X. Shen, Science **325**, 178 (2009).

[4] D. Hsieh, Y. Xia, D. Qian, L. Wray, J. H. Dil, F. Meier, J. Osterwalder, L. Patthey, J. G. Checkelsky, N. P. Ong, A. V. Fedorov, H. Lin, A. Bansil, D. Grauer, Y. S. Hor, R. J. Cava, and M. Z. Hasan, Nature (London) **460**, 1101 (2009).

[5] L. Fu, C. L. Kane, and E. J. Mele, Phys. Rev. Lett. **98**, 106803 (2007).

[6] S. Murakami, N. Nagaosa, and S. C. Zhang, Phys. Rev. Lett. **93**, 156804 (2004).

[7] M. König, S. Wiedmann, C. Brüne, A. Roth, H. Buhmann, L. W. Molenkamp, X.-L. Qi, and S.-C. Zhang, Science **318**, 766 (2007).

[8] L. Fu, Phys. Rev. Lett. **106**, 106802 (2011).

[9] Y. Tanaka, Z. Ren, T. Sato, K. Nakayama, S. Souma, T. Takahashi, K. Segawa, and Y. Ando, Nat. Phys. **8**, 800 (2012).

[10] S. M. Young, S. Zaheer, J. C. Y. Teo, C. L. Kane, E. J. Mele, and A. M. Rappe, Phys. Rev. Lett. **108**, 140405 (2012).

[11] Z. K. Liu, B. Zhou, Y. Zhang, Z. J. Wang, H. M. Weng, D. Prabhakaran, S.-K. Mo, Z. X. Shen, Z. Fang, X. Dai, Z. Hussain, and Y. L. Chen, Science **343**, 864 (2014).

[12] A. H. Castro Neto, F. Guinea, N. M. R. Peres, K. S. Novoselov, and A. K. Geim, Rev. Mod. Phys. **81**, 109 (2009).

[13] S. Das Sarma, S. Adam, E. H. Hwang, and E. Rossi, Rev. Mod. Phys. **83**, 407 (2011).

[14] M. Z. Hasan and C. L. Kane, Rev. Mod. Phys. **82**, 3045 (2010).

[15] X. L. Qi and S. C. Zhang, Rev. Mod. Phys. **83**, 1057 (2011).

[16] C.-Z. Chang, J. Zhang, X. Feng, J. Shen, Z. Zhang, M. Guo, K. Li, Y. Ou, P. Wei, L.-L. Wang, Z.-Q. Ji, Y. Feng, S. Ji, X. Chen, J. Jia, X. Dai, Z. Fang, S.-C. Zhang, K. He, Y. Wang, L. Lu, X.-C. Ma, and Q.-K. Xue, Science **340**, 167 (2013).

[17] W. K. Tse, Z. Qiao, Y. Yao, A. H. MacDonald, and Q. Niu, Phys. Rev. B. **83**, 155447 (2011).

[18] X. Du, I. Skachko, F. Duerr, A. Luican, and E. Y. Andrei, Nature (London) **462**, 192 (2009).

[19] A. A. Burkov, Phys. Rev. Lett. **113**, 247203 (2014).

[20] A. A. Zyuzin and A. A. Burkov, Phys. Rev. B **86**, 115133 (2012).

[21] L. Fu and C. L. Kane, Phys. Rev. Lett. **100**, 096407 (2008).

[22] A. R. Akhmerov, J. Nilsson, and C. W. J. Beenakker, Phys. Rev. Lett. **102**, 216404 (2009).

[23] L. Li, Y. Yu, G. Ye, Q. Ge, X. Ou, H. Wu, D. Feng, X. Chen, and Y. Zhang, Nat. Nanotechnol. **9**, 372 (2014).

[24] H. Liu, A. T. Neal, Z. Zhu, Z. Luo, X. Xu, D. Tomanek, and P. D. Ye, ACS Nano **8**, 4033 (2014).

[25] F. Xia, H. Wang, and Y. Jia, Nat. Commun. **5**, 5458 (2014).

[26] V. Tran, R. Soklaski, Y. Liang, and L. Yang, Phys. Rev. B **89**, 235319 (2014).

[27] R. Fei and L. Yang, Nano Lett. **14**, 2884 (2014).

[28] R. Fei, A. Faghaninia, R. Soklaski, J.-A. Yan, C. Lo, and L. Yang, Nano Lett. **14**, 6393 (2014).

[29] X. Wang, A. M. Jones, K. L. Seyler, V. Tran, Y. Jia, H. Zhao, H. Wang, L. Yang, X. Xu, and F. Xia, Nat. Nanotechnol (2015).

[30] Z. Zhu and D. Tomanek, Phys. Rev. Lett. **112**, 176802 (2014).

[31] V. Tran and L. Yang, Phys. Rev. B **89**, 245407 (2014).

[32] A. S. Rodin, A. Carvalho, and A. H. Castro Neto, Phys. Rev. Lett. **112**, 176801 (2014).

[33] L. Liang, J. Wang, W. Lin, B. G. Sumpter, V. Meunier, and M. Pan, Nano Lett. **14**, 6400 (2014).

[34] R. W. Keyes, Phys. Rev. **92**, 580 (1953).

[35] J. P. Perdew, K. Burke, and M. Ernzerhof, Phys. Rev. Lett. **77**, 3865 (1996).

[36] S. Grimme, J. Comput. Chem. **25**, 1463 (2004).

[37] J. Heyd, G. E. Scuseria, and M. Ernzerhof, J. Chem. Phys. **118**, 8207 (2003).

[38] J. Heyd, G. E. Scuseria, and M. Ernzerhof, J. Chem. Phys. **124**, 219906 (2006).

[39] X. Y. Zhou, R. Zhang, J. P. Sun, Y. L. Zou, D. Zhang, W. K. Lou, F. Cheng, G. H. Zhou, F. Zhai, and K. Chang, arXiv:1411.4275.

[40] M. Ezawa, New J. Phys. **16**, 115004 (2014).

[41] I. Zutic, J. Fabian, and S. D. Sarma, Rev. Mod. Phys. **76**, 323 (2004).

[42] X. Qian, J. Liu, L. Fu, and J. Li, Science **346**, 1344 (2014).

[43] F. Guinea, M. I. Katsnelson, and A. K. Geim, Nat. Phys. **6**, 30 (2010).

[44] H. Zhang, C.-X. Liu, X.-L. Qi, X. Dai, Z. Fang, and S.-C. Zhang, Nat. Phys. **5**, 438 (2009).

[45] Q. Liu, X. Zhang, L. B. Abdalla, A. Fazzio, and A. Zunger, Nano Lett. **15**, 1222 (2015).

[46] See Supplemental Material at http://link.aps.org/supplemental/10.1103/PhysRevB.91.195319 for details of the evolution of band gaps, effective mass, and carrier mobilities of BP under pressure. The effect of the atomic distortion on the relaxed structures is presented as well.

[47] Q. Wei and X. Peng, Appl. Phys. Lett. **104**, 251915 (2014).

[48] Y. Katayama, T. Mizutani, W. Utsumi, O. Shimomura, M. Yamakata, and K. Funakoshi, Nature (London) **403**, 170 (2000).

[49] G. Monaco, S. Falconi, W. A. Crichton, and M. Mezouar, Phys. Rev. Lett. **90**, 255701 (2003).

[50] R. R. Nair *et al.*, Science **320**, 1308 (2008).

[51] Z. J. Xiang, G. J. Ye, C. Shang, B. Lei, N. Z. Wang, K. S. Yang, D. Y. Liu, F. B. Meng, X. G. Luo, L. J. Zou, Z. Sun, Y. B. Zhang, and X. H. Chen, arXiv:1504.00125.

[52] G. Kresse and J. Furthmüller, Phys. Rev. B. **54**, 11169 (1996).